Ocean Modelling xxx (2009) xxx–xxx

Contents lists available at ScienceDirect

Ocean Modelling

journal homepage: www.elsevier.com/locate/ocemod

An unstructured C-grid based method for 3-D global ocean dynamics: Free-surface formulations and tidal test cases

G.R. Stuhne *, W.R. Peltier

Department of Physics, University of Toronto, 60 St. George Street, Toronto, Ont., Canada M5S 1A7

ARTICLE INFO

Article history:
Received 23 April 2008
Received in revised form 27 October 2008
Accepted 20 November 2008
Available online xxxx

Keywords:
Ocean modeling
Unstructured grids

ABSTRACT

In an earlier work, we described how an unstructured grid numerical framework based on an energy-conserving Arakawa C-grid discretization could be applied to ocean general circulation models (OGCMs). We discuss herein how we adapted our previously published rigid-lid, hydrostatic, Boussinesq OGCM techniques to shallow-water and baroclinic free-surface dynamics. The simulation of the global M_2 tide is proposed as a useful benchmark for testing unstructured grid ocean models. Tidal simulations are much more manageable that full-fledged OGCM climate simulations, being based on simpler physical assumptions and parameterizations, and requiring less computation time per test. We demonstrate that the results of unstructured Arakawa C-grid simulations of the M_2 tide reproduce those of an equivalent regular grid discretization. Because unstructured grid methods carry a computational overhead, however, their use can only be justified where resolution must be concentrated in localized regions. The tides around Hudson's Bay are well-described in a multi-scale context, and we show that strong discontinuities in mesh resolution do not appreciably distort the shallow-water tidal solution. Progressing to fully 3-D models, it is demonstrated that the barotropic M_2 tidal structure is consistently represented between models. Efforts to resolve the generation of baroclinic waves by the barotropic tide were, however, frustrated by the existence of a numerical mode that has been independently verified by other investigators working on similar methods. This presents a challenge for future work.

1. Introduction

In a previous paper (Stuhne and Peltier, 2006, hereafter SP), we described a new numerical framework for unstructured grid ocean modeling on a global scale. Prior to that work, the published applications of unstructured meshes to oceanography had been restricted to smaller scale coastal and tidal modeling (see, e.g. Myers and Weaver, 1995; Lynch et al., 1996; Casulli and Walters, 2000; Chen et al., 2003; Nechaev et al., 2003; Zhang et al., 2004). A number of potential advantages motivated us to extend this promising numerical technology to the simulation of the global ocean. For one thing, the global ocean circulation is affected by dynamics on many scales, and some localized small-scale processes exert inordinate influence on the system as a whole. Western boundary currents like the Gulf Stream are a case in point. It is a clear benefit to be able to increase mesh resolution in local regions of interest, without having to resolve the entire global domain finely enough to accommodate the smallest simulated features. Apart from some basic grid stretching and remapping techniques (e.g., Murray, 1996), traditional regular grid ocean general circulation models (OGCMs) inspired by the early efforts of Bryan (1969) and Bryan and Cox (1972) offer few options in this regard. Unstructured grid techniques are, on the other hand, naturally suited to multi-scale modeling.

One of the problems that motivated this work is that of global climate modeling, which raises many issues relating to multiple scales and localized regions of interest. For instance, the concentration of the northern sea-ice mass in the narrow channels of the Arctic archipelago can have a great impact on climate because of the effects on the global thermohaline circulation (THC). The work reported in SP included results from 3-D, 5-year annually forced simulations of the global ocean, whose climatological spin-up was captured with rudimentary success. The mathematical model that was adopted built upon the coastal modeling work of Casulli and Walters (2000), which was extended into an energy-conserving, fully spherical, z-coordinate, rigid-lid hydrostatic Boussinesq model with temperature and salinity tracers. This dynamical system was discretized on an Arakawa (1966) C-type horizontal grid, using a spherical shell version of the Perot (2000) projection scheme for the momentum equation. The use of the projection makes it possible to preserve quadratic invariants (squared temperature and salinity, as well as total energy) to arbitrarily prescribed accuracy.

Subsequent to the publication of SP, a somewhat similar non-spherical and non-hydrostatic model was described by

* Corresponding author. Tel.: +1 416 946 3019.
E-mail address: gordan@atmosp.physics.utoronto.ca (G.R. Stuhne).

1463-5003/$ - see front matter © 2008 Elsevier Ltd. All rights reserved.
doi:10.1016/j.ocemod.2008.11.005

Fringer et al. (2006), who followed Casulli and Walters (2000) in applying it to small-scale coastal modeling problems. This model, named SUNTANS by the authors, is less stringent about maintaining energy conservation, which imposes a computational cost during C-grid implicit time stepping. Although the two methodologies should produce comparable results in practice, ours is more theoretically rigorous, and the quantitative degree of energy conservation can be tuned down and compromised when greater efficiency is desired. The ability to control the conservation properties of the methods of SP should be a significant advantage in the validation of climate-type simulations, in which the numerical drift of invariants can have serious long-term effects. Beyond the conservation issue, Fringer et al. (2006) did also implement a few relevant features that we did not address in SP. Most significantly, SUNTANS can accommodate an implicit linear free surface when a hydrostatic constraint is activated. We will describe below how these dynamics are implemented in our scheme, which applies to fully spherical geometry. Overall, our work fills an important gap in the literature about the Arakawa C-grid family of methods, which have not previously been applied to the large-scale, coarsely resolved problems of climate dynamics.

Rather than grapple with numerical issues in the climatological context, where test runs take a very long time and results depend upon elaborate *ad hoc* assumptions, we shifted our attention to the simpler problem of simulating the global tides. Tidal dynamics also exhibit multiple geometry-induced scales and a rich range of barotropic and baroclinic phenomena, but play out on a time-scale of days, as opposed to years and decades. At the same time, the simple *a priori* assumptions behind tidal analyses have long been well understood, while the observational data sets that are available for comparison purposes are constantly improving (see, e.g., Egbert and Ray, 2003 and references). All of these factors make the problem of tidal simulation an ideal benchmark for testing new global unstructured grid ocean models. In this study, we will focus exclusively on the case of the global M_2 tide, which has been extensively analyzed and observed.

Since the leading-order tidal response is linear and well represented even by shallow-water dynamics, comparisons can begin in this regime, and then evolve through increasing levels of sophistication, i.e.: nonlinearity, new parameterizations, three-dimensionality, stratification, etc. (e.g., Gill, 1982). It would be a great success for a global unstructured grid tidal circulation model, if it were able to capture the local production of baroclinic waves by the barotropic tide. This problem has been addressed in the context of local, high resolution finite element models (e.g., Hall and Davies, 2005), but global simulations have been carried out successfully only fairly recently, even in the structured grid context (see Simmons et al., 2004). There are still many open issues of physics that a multi-scale unstructured grid modeling framework might help to resolve. We have not yet attained this goal with our own methods, but we present a sequence of analyses that helps to frame the problem.

The numerical methods described in SP did not represent the dynamics of the free surface of the ocean, a feature that is clearly essential for any kind of barotropic tidal simulation. In Section 2, we introduce a suitably generalized version of the numerical structure, along with the simple mathematical tidal model that is being assumed. Extensive background discussion pertaining to the original numerical methods of SP and the model assumptions will not be provided here, and the reader will instead be directed to the relevant literature. In Section 3, a progression of test simulations will be discussed, while conclusions and future directions will be addressed in Section 4.

2. Model and numerical discretization

2.1. Dynamical equations

The most general dynamical model that is utilized in the present study makes use of the same hydrostatic and Boussinesq approximation as SP. These assumptions pertain to the interior of the fluid, while the addition of the free surface dynamics pertains to the upper boundary condition, which is considered below in Section 2.2. In the present study, we can make do with using a simple density representation of the scalar dynamics, so the equation of state in the hydrostatic balance constraint becomes trivial. Assuming a non-dimensionalization whose respective length and time units are r_0 and $2\pi/\Omega_0$ (r_0 being the radius of the Earth at sea level, and Ω_0 being the planetary rotation rate), then the hydrostatic condition relating ρ to pressure, p, has the form

$$\frac{4\pi^2}{\Omega_0^2 r_0 \rho_0}(\hat{\mathbf{r}}\cdot\nabla p + g\rho) = \frac{\partial \hat{p}}{\partial z} + \hat{\rho} = 0, \tag{1}$$

in which $z \equiv \sqrt{x^2+y^2+z^2} - 1$ is the offset vertical coordinate, $\hat{\mathbf{r}}$ is the local radial basis vector, ρ_0 is the Boussinesq background density and g is the acceleration due to gravity.

We work in a general regular coordinate representation in which total fluid velocity is $v = v_x\hat{\mathbf{x}} + v_y\hat{\mathbf{y}} + v_z\hat{\mathbf{z}}$, while vertical and horizontal fluid velocities are defined, respectively, as $w \equiv v\cdot\hat{\mathbf{r}}$ and $\mathbf{u} \equiv v - w\hat{\mathbf{r}}$. With these definitions in place, the Boussinesq volume conservation condition and advection operator are given by

$$\nabla\cdot v = \nabla\cdot\mathbf{u} + \frac{\partial w}{\partial z} = 0 v\cdot\nabla = \mathbf{u}\cdot\nabla + w\frac{\partial}{\partial z}, \tag{2}$$

and we can write down the prognostic dynamical equations for the interior of the fluid volume: i.e.,

$$\begin{aligned} &\frac{\partial \mathbf{u}}{\partial t} + [v\cdot\nabla - \mathscr{D}(\nu_h,\nu_v) + 4\pi\hat{\mathbf{z}}\times]\mathbf{u} + \nabla p = \mathbf{F}_\mathbf{u} + \Lambda\hat{\mathbf{r}} \\ &\frac{\partial \rho}{\partial t} + \left[v\cdot\nabla - \mathscr{D}(\mu_h,\mu_v)\right]\rho = 0. \end{aligned} \tag{3}$$

$\mathscr{D}(\kappa,\sigma)$ in Eq. (3) is a schema for a linear diffusion operator with respective horizontal and vertical diffusivities κ and σ. The coefficients ν_h, ν_v, μ_h and μ_v can in general vary in space and time according to complex parameterizations, but for purposes of the present study they can be assumed constant. Meanwhile, Λ is a Lagrangian multiplier for a constraint force that must act to keep fluid particles confined to a spherical shell when $w = 0$ and $v = \mathbf{u}$ (see Cøté (1988) and SP for a discussion of this). Since the discretization implicitly introduces constraints, we do not need to worry about the specific form of Λ. The remaining term in Eq. (3), $\mathbf{F}_\mathbf{u}$, pertains to the forcing on the momentum equation, and is considered in the following subsection.

2.2. Boundary conditions and the shallow water model (SWM)

The surface boundary condition is determined by the integrated 3-D continuity equation, which has the form

$$\frac{\partial \eta}{\partial t} + \nabla\cdot\mathbf{U} = 0, \tag{4}$$

in which the net horizontal flux, $\mathbf{U}$, is the vertically integrated horizontal velocity: i.e.,

$$\mathbf{U} \equiv \int_{-H}^{\eta} \mathbf{u}\,dz. \tag{5}$$

A linear free surface results when η is set to 0 in Eq. (5), and a rigid lid condition can then be imposed if one also sets $\frac{\partial\eta}{\partial t} = 0$ in Eq. (4).

Please cite this article in press as: Stuhne, G.R., Peltier, W.R., An unstructured C-grid based method for 3-D global ocean dynamics: ..., Ocean Modell. (2009), doi:10.1016/j.ocemod.2008.11.005

Eqs. (3)–(5) determine the SWM if we set $\rho = \rho_c$ and

$$\mathbf{u} = v = \frac{\mathbf{U}}{H+\eta}$$

for a single layer of fluid, which gives us the following form of the momentum equation, i.e.:

$$\frac{\partial \mathbf{u}}{\partial t} + [\mathbf{u}\cdot\nabla - \mathscr{D}(v_h, v_v) + 4\pi\hat{\mathbf{z}}\times]\mathbf{u} + \rho_c\nabla\eta = \mathbf{F}_\mathbf{u} + \Lambda\hat{\mathbf{r}}. \tag{6}$$

2.3. Tidal forcing and dissipation

The form of the forcing function in Eqs. (3) and (6) is given by

$$\mathbf{F}_\mathbf{u} = -\nabla(\rho\eta_*) + \mathbf{F}_\mathbf{u}^{\text{bott}}, \tag{7}$$

in which η_* has the form

$$\eta_* = \gamma\eta + \frac{A_{M_2}\sqrt{1-z^2}(y\cos\Omega_{M_2}t - x\sin\Omega_{M_2}t)}{\sqrt{x^2+y^2}}, \tag{8}$$

corresponding to the standard M_2 tidal forcing function (amplitude and period A_{M_2} and Ω_{M_2}, respectively) with a self-attraction and loading term (coefficient γ). The bottom stress is represented in Eq. (7) as a volume forcing over a boundary layer of height δz, giving

$$\mathbf{F}_\mathbf{u}^{\text{bott}} = \begin{cases} \frac{-c_d u_d(|\mathbf{u}|)\mathbf{u}}{\delta z} & \text{for } -H \leqslant z \leqslant -H+\delta z \\ 0 & \text{elsewhere.} \end{cases} \tag{9}$$

If δz is the height of the discrete computational element above the lower boundary, then Eq. (9) is equivalent to a finite difference representation of a bottom drag stress with coefficient c_d. The bottom drag can be nonlinear (with $u_d(|\mathbf{u}|) = |\mathbf{u}|$) or linear (with $u_d(|\mathbf{u}|) = U_*$, for constant U_*).

2.4. Discretization

The discretization of the rigid-lid model was described in great detail in SP, wherein we developed an algebraic notation scheme for expressing the discrete equations in compact form. Since the basic numerical structure is still the same, we will, in what follows, discuss high-level expressions while omitting most of the details about how these translate into basic arithmetical operations. A basic summary is provided in this section, and readers requiring further information are directed to our earlier paper.

We begin by writing down the space-time discretization of the 3-D baroclinic model. The evolution equations for horizontal velocity, u, density, ρ, and surface displacement, η, have the following high-level form: i.e.,

$$\begin{aligned} &\frac{u^{r+1}-u^r}{\Delta t} + \vec{\Gamma}^{-1}\cdot\{[\mathscr{L}(u^r, v_h, v_v) + 4\pi\hat{\mathbf{z}}\times]\vec{\Gamma}u^{r+\frac{1}{2}} - \mathbf{F}_\mathbf{u}^r\} = -\frac{\Delta p^{r+\frac{1}{2}}}{|\Delta\mathbf{X}|} \\ &\frac{\rho^{r+1}-\rho^r}{\Delta t} + \mathscr{L}(u^r, \mu_h, \mu_v)\rho^{r+\frac{1}{2}} = 0 \\ &\frac{\eta^{r+1}-\eta^r}{\Delta t} = w_{z=0}^{r+\frac{1}{2}}. \end{aligned} \tag{10}$$

The superscript r specifies the time-level at which a quantity is evaluated, with $\chi^{r+\frac{1}{2}}$ denoting the average $\frac{1}{2}(\chi^r + \chi^{r+1})$ and Δt being the time-step size. The operators $\vec{\Gamma}$ and $\vec{\Gamma}^{-1}$ are defined below in Eq. (11).

The dynamical fields are evaluated on an Arakawa C-grid with a prismatic z-coordinate representation of the vertical structure. The bathymetry is approximated by bottom truncation and boundaries between vertical levels are everywhere at the same depth, although layers may have varying thickness. In SP, we described an indexing system in which $\mathbf{x}_i$ denotes the position of the i^{th} horizontal node, while the schemas $\lambda_{\mathbf{e},m} = \lambda_{(e_1,e_2),m}$ and $\Phi_{\mathbf{c},m} = \Phi_{(c_1,c_2,c_3),m}$ are used to denote quantities attached to the m^{th} vertical level, to edges and triangles, respectively. The index components e_j and c_j indicate the endpoints of edges and corners of triangles, respectively.

The topology and geometry are illustrated, for the horizontal and vertical grids, in the respective Figs. 1 and 2. The fields $\mathbf{X}_{(c_1,c_2,c_3)}$ and $\bar{\mathbf{x}}_{(e_1,e_2)}$ denote, respectively the circumcenters of triangular faces and the midpoints of edges. In the 3-D prismatic schema, horizontal velocity u is represented in terms of its normal components at the rectangular horizontal faces of prisms, while density, ρ, and pressure, p, reside at the circumcenters of the prisms. Vertical velocity, w, is evaluated at the vertical triangular faces and the time derivative of the surface displacement, η, is therefore associated with the surface upwelling velocity, $w_{z=0}$.

Eq. (10) contains a number of schematic operators that act on cell and edge fields. The difference operator, $\Delta\Phi$, evaluated at an

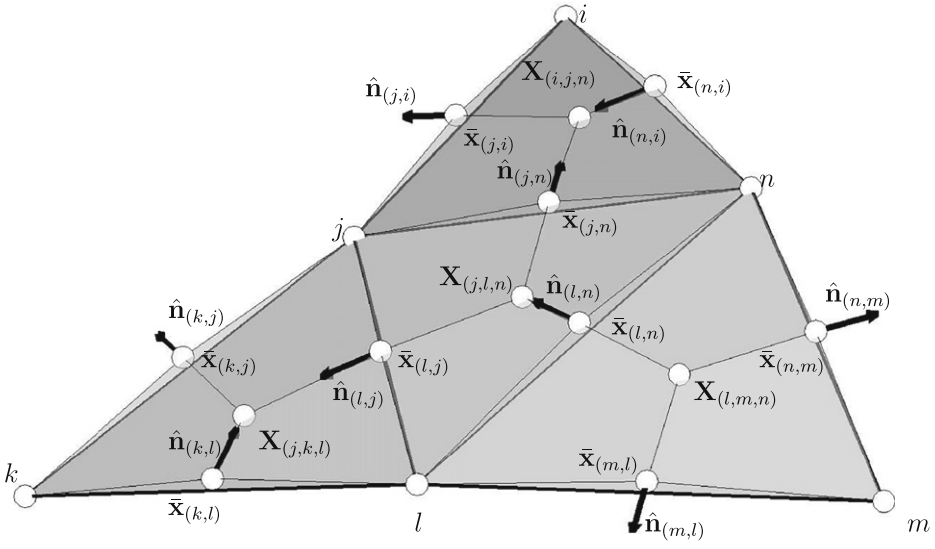

Fig. 1. A representation of four neighboring surface triangles that illustrates the indexing scheme, as well as some relevant geometric quantities (nodes, edge midpoints and normals, and face circumcenters). Reproduced from SP.

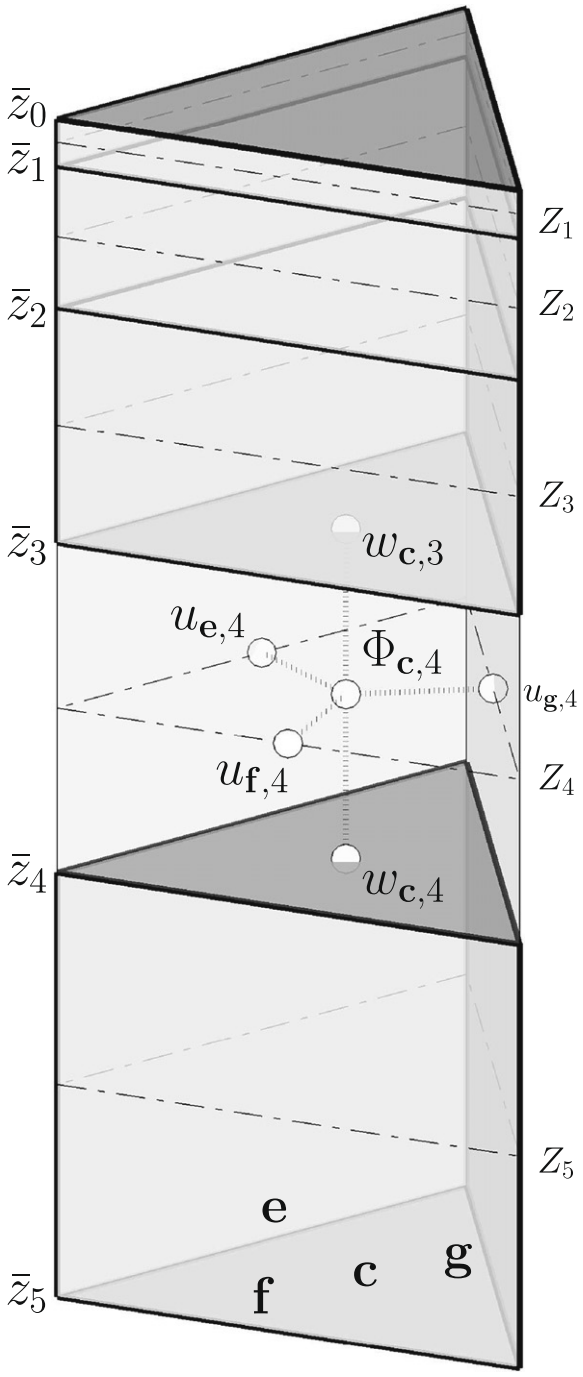

Fig. 2. Radial discretization of a column beneath a cell, c, and its adjacent edges, e–g. Reproduced from SP.

edge, denotes the difference between the values of Φ at the two circumcenters adjacent to the edge. Meanwhile, if $\mathbf{F}$ is a vector field evaluated at circumcenters and $F^{\perp}$ is an approximation in terms of edge normals, then the action of the operators $\vec{\Gamma}$ and $\vec{\Gamma}^{-1}\cdot$ is to sustain the following approximations, i.e.:

$$\begin{aligned}\mathbf{F} &\approx \vec{\Gamma}F^{\perp} \equiv \frac{\mathbf{X}\Delta^T(\ell F^{\perp}) - \Delta^T(\ell\bar{\mathbf{x}}F^{\perp})}{A}\\ F^{\perp} &\approx \vec{\Gamma}^{-1}\cdot\mathbf{F} \equiv \frac{\Delta(\mathbf{X}\cdot\mathbf{F}) - \bar{\mathbf{x}}\cdot\Delta\mathbf{F}}{|\Delta\mathbf{X}|},\end{aligned} \tag{11}$$

in which A and ℓ denote triangle areas and edge lengths, respectively, while Δ^T denotes the transpose of the difference operator, Δ. The theoretical basis for Eq. (11), which generalize the projection scheme of Perot (2000), is explained in SP, wherein it is demonstrated how the quadratic norm of the vector field is preserved under transformation between the circumcentral and edge-normal representations.

Another operator schema that was introduced in Eq. (10) pertains to the discretization of the material conservation law under advection and diffusion, i.e.:

$$\begin{aligned}\mathscr{L}(u,\kappa,\sigma)\Phi &\equiv -\frac{1}{A}\Delta^T\left(\ell u\langle\Phi\rangle - \ell\kappa\frac{\Delta\Phi}{|\Delta\mathbf{X}|}\right) - \frac{\Delta_z^T}{\Delta_z^T\bar{z}}\left(w\langle\Phi\rangle_z - \sigma\frac{\Delta_z\Phi}{\Delta_z Z}\right)\\ \mathscr{L}(u,0,0)1 &= -\frac{1}{A}\Delta^T(\ell u) - \frac{\Delta_z^T w}{\Delta_z^T\bar{z}} = 0,\end{aligned} \tag{12}$$

in which Z, $\bar{z}$, Δ_z, and Δ_z^T are defined to be the simpler, vertical analogues of $\mathbf{X}$, $\bar{\mathbf{x}}$, Δ, and Δ^T, respectively, while $\langle\cdot\rangle$ and $\langle\cdot\rangle_z$ schematize the respective horizontal and vertical averaging of values adjacent to faces.

The second equation in (12) corresponds to the application of the general schema to the identity field, which furnishes the discretized Boussinesq non-divergence condition that enables w to be determined in terms of u by vertical integration.

The implicit time evolution equation for density in (10) has the same form as the scalar evolution equations in SP, i.e.:

$$\left[1+\tfrac{\Delta t}{2}\mathscr{L}(u^r,\mu_h,\mu_v)\right]\rho^{r+1} = \left[1-\tfrac{\Delta t}{2}\mathscr{L}(u^r,\mu_h,\mu_v)\right]\rho^r + \Delta t F_\rho^r, \tag{13}$$

and the discrete algebraic problem is solved with the aid of the GMRES algorithm implemented by CERFACS (Frayss et al., 2003). Once the iteration for ρ^{r+1} is performed, $\rho^{r+\frac{1}{2}} = \frac{1}{2}(\rho^r + \rho^{r+1})$ can be used to determined the pressure from the hydrostatic balance condition,

$$\Delta_z p = -\langle\rho\Delta_z^T\bar{z}\rangle_z, \tag{14}$$

given the boundary condition for surface pressure, i.e.:

$$p_s = p_{m=0} = \rho_s^{r+\frac{1}{2}}\eta, \tag{15}$$

in which ρ_s is the surface density.

The algebraic problem for advancing the coupled η and u fields is analogous to Eq. (13), but considerably more complex. Using a schematic form similar to that introduced in SP for the rigid-lid problem, we get the following discrete system:

$$\left[\mathscr{I}+\frac{\Delta t}{2}\mathscr{P}^r\right]\begin{bmatrix}u^{r+1}\\ \eta^{r+1}\end{bmatrix} = \left[\mathscr{I}-\frac{\Delta t}{2}\mathscr{P}^r\right]\begin{bmatrix}u^r\\ \eta^r\end{bmatrix} + \Delta t\begin{bmatrix}\vec{\Gamma}^{-1}\cdot\mathbf{F}_{\mathbf{u}}^r - \frac{\Delta p_h^{r+\frac{1}{2}}}{|\Delta\mathbf{X}|}\\ 0\end{bmatrix}, \tag{16}$$

where $\mathscr{I}$ is the identity operator and

$$\mathcal{P}^r \equiv \left[\begin{array}{c|c}\vec{\Gamma}^{-1}\cdot\left\{\left[\mathcal{L}\left(u^r,\nu_h,\nu_v\right)+4\pi\hat{\mathbf{z}}\times\right]\vec{\Gamma}\ldots\right\} & \frac{\Delta}{|\Delta\mathbf{X}|}\left(\rho_s^{r+\frac{1}{2}}\ldots\right)\\ \hline \sum_m\left\{\Delta_z^T\bar{z}\Delta^T\left[\ell\ldots\right]\right\}_m & 0\end{array}\right]. \tag{17}$$

Comparison with SP will verify that this expression is much cleaner and more symmetric than the version with the rigid-lid constraint, and Eqs. (16) and (17) yield a better-conditioned matrix problem in the limit of small time-steps. As in SP, the GMRES algorithm can be used to iteratively solve for u^{r+1} and η^{r+1}.

3. Numerical tests

3.1. Mesh generation and bathymetry

In an unstructured grid context, there is a need for relatively sophisticated techniques for generating meshes, assimilating data

Please cite this article in press as: Stuhne, G.R., Peltier, W.R., An unstructured C-grid based method for 3-D global ocean dynamics: ..., Ocean Modell. (2009), doi:10.1016/j.ocemod.2008.11.005

such as bathymetry, and then consolidating these elements into an executable simulation code whose results can subsequently be analyzed. A number of the issues have been addressed in SP, and since then a new software framework has been developed to organize and structure the various tasks in an integrated framework. Script-based setup tools backed up by a graphical user interface have been designed with the goals of facilitating the re-use of software components while avoiding situations where older analyses become orphaned and un-reproducible due to the evolution of the system.

A full technical explanation of the mesh setup procedures and the analysis software is beyond the scope of this paper. We mention, however, that, as in SP, the global unstructured grids for the test cases are generated by a quadtree method beginning with a basic spherical icosahedron. Bathymetry is again based on the ETOPO2 data set National Geophysical Data Center (NGDC), 2001.

3.2. Protocols

To assess the skill of the numerical methods, a progression of tidal test simulations is analyzed and compared against the results of a generic regular grid scheme that has been locally implemented by Griffiths and Peltier (2008) for purposes of analyzing tidal effects at last glacial maximum. Beyond the fact that results were conveniently available, this work was a useful basis for comparison because of the numerical technique being based on a second-order Arakawa C-grid spatial discretization. This is the direct regular grid analogue of our unstructured grid scheme, except that formal second-order accuracy is seen in SP to be lost with grid non-uniformity.

An essentially constant protocol is used to perform and analyze all of the unstructured grid tidal simulations. In integrating the dynamical equations, we use standard values (see, e.g., Gill, 1982) of $A_{M_2} = 0.34504$ m and $\Omega_{M_2} = 1.405 \times 10^{-3}$ s^{-1} for the tidal amplitude and frequency along with a drag coefficient of $c_d = 2.5 \times 10^{-3}$. When bottom drag is linearized, a characteristic velocity of $U_* = 1.0$ m/s is assumed. Unless otherwise specified with respect to particular results, the tidal equations were integrated forward in time for 20 tidal periods (approximately 10 days), which is sufficient to achieve a periodic response in the linear barotropic mode. For purposes of comparison, standard methods are used to interpolate the tidal surface displacement, η, onto latitude-longitude grids, enabling results to be easily depicted in the form of amplitude-phase plots. Additional aspects of the various solutions will be plotted when the discussion warrants.

3.3. Shallow-water dynamics

Resolving the global barotropic signal induced by tidal forcing requires at least a linearized shallow-water dynamical system. Given the linear and perturbative nature of the problem, these simplified equations are, even in recently published work (e.g., Egbert and Ray, 2003), often sufficient for the analysis of tidal physics. In Fig. 3, we show linear amplitude and phase results obtained according to the protocols of Section 3.2, and with a uniform unstructured grid of approximately uniform 0.5° node spacing over the globe. The grid was generated as a level 7 quadtree refinement

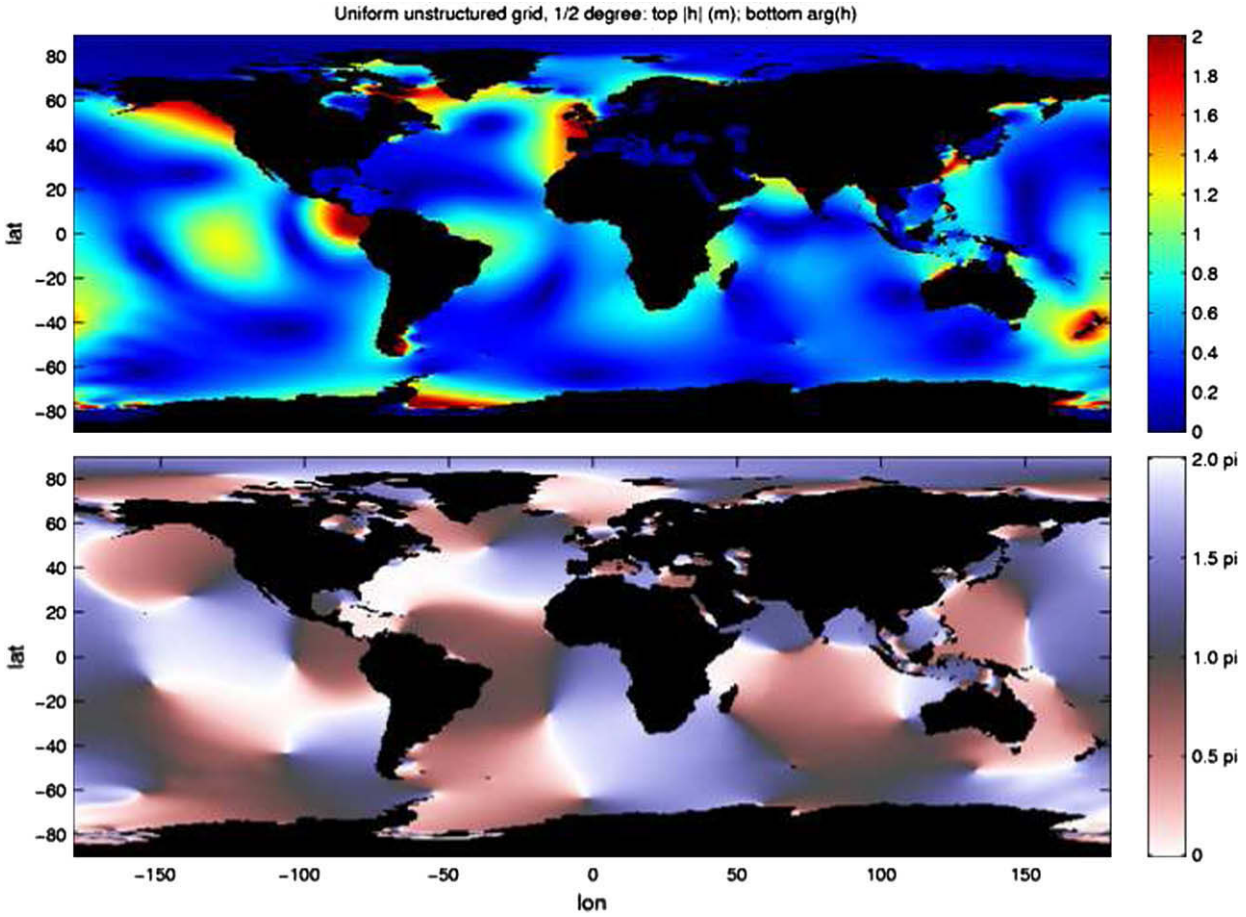

Fig. 3. Amplitude and phase plots from an equilibrated linear M_2 tidal simulation performed on a uniform level 7 (approximately $1/2^0$) global icosahedral quadtree grid.

Please cite this article in press as: Stuhne, G.R., Peltier, W.R., An unstructured C-grid based method for 3-D global ocean dynamics: ..., Ocean Modell. (2009), doi:10.1016/j.ocemod.2008.11.005

of the spherical icosahedron. Considering that regular grid resolution becomes finer at higher latitudes, this is comparable, overall, to a latitude-longitude grid having 2/3° node spacing at the equator. Results from such a grid are shown in Fig. 4 for comparison. The point to note is that the plots are essentially identical, which is the hoped for result.

The case just described confirms the theoretical principle that unstructured Arakawa C-grid tidal simulations should, with nearly uniform grids in a 2-D shallow-water context, be as accurate as analogous regular grid results. Under uniform conditions, however, regular grids must be preferred because the linear array structure of field data facilitates greater efficiency, especially on vector processors. We did not optimize the code sufficiently to make reliable quantitative comparisons, but it is reasonable to estimate from our findings that unstructured grid simulations are, under identical uniform grid conditions, an order of magnitude slower. This extra investment of numerical resources can only be recouped if the unstructured grid is used in a multi-scale context, in such a way as to deliver locally enhanced resolution when a global regular grid simulation at that resolution would be impractical.

Considering that unstructured grids will only be practically useful in multi-scale contexts, we repeat the simulation whose results are shown in Fig. 5 with an unstructured grid containing sharp resolution jumps. As discussed in SP and elsewhere, strong gradients in mesh resolution and the attendant poorly shaped elements result in a degradation to first-order accuracy. This may cause problems as energetic small-scale Kelvin and gravity waves propagate into regions of the mesh where they cease to be resolved. The best way to assess whether this is occurring is by qualitative examination of the solution in the vicinity of the resolution discontinuities. Since defects would not show up clearly in interpolated global amplitude and phase plots, we instead examine the height field solution at a fixed time level plotted directly onto an unstructured mesh.

The local grid view shown in Fig. 5 has a relatively large region about Hudson's Bay in which the resolution is increased to quadtree level 8 (about 1/4°), leaving a sharp discontinuity in resolution at the boundary with the global level 7 grid. An inner region encompassing most of the Bay and some of the small inlets and channels in its northern reaches is further refined to level 9 (about 1/8°), leaving another sharp resolution jump. In spite of this sub-optimal grid structure, however, the contour plots of height in the ±1 m range (with 0.1 m contour spacing) show no evidence of any distortions tied to the grid. Instead, the advantages of an unstructured grid multi-resolution approach in tidal modeling are highlighted by the small-scale regions of high activity in channels and inlets that would not appear in the global level 7 grid.

The results plotted in Fig. 5 demonstrate that sharp resolution gradients do not, in and of themselves, compromise shallow-water tidal simulations in practically appreciable ways. It should be noted, however, that circumcentral Arakawa C-grids of the type that we are using can, without due diligence, easily incorporate element pairs whose circumcenters collapse to a common point, and this produces pathological inaccuracies. The software suite that we have developed to generate grids incorporates a number

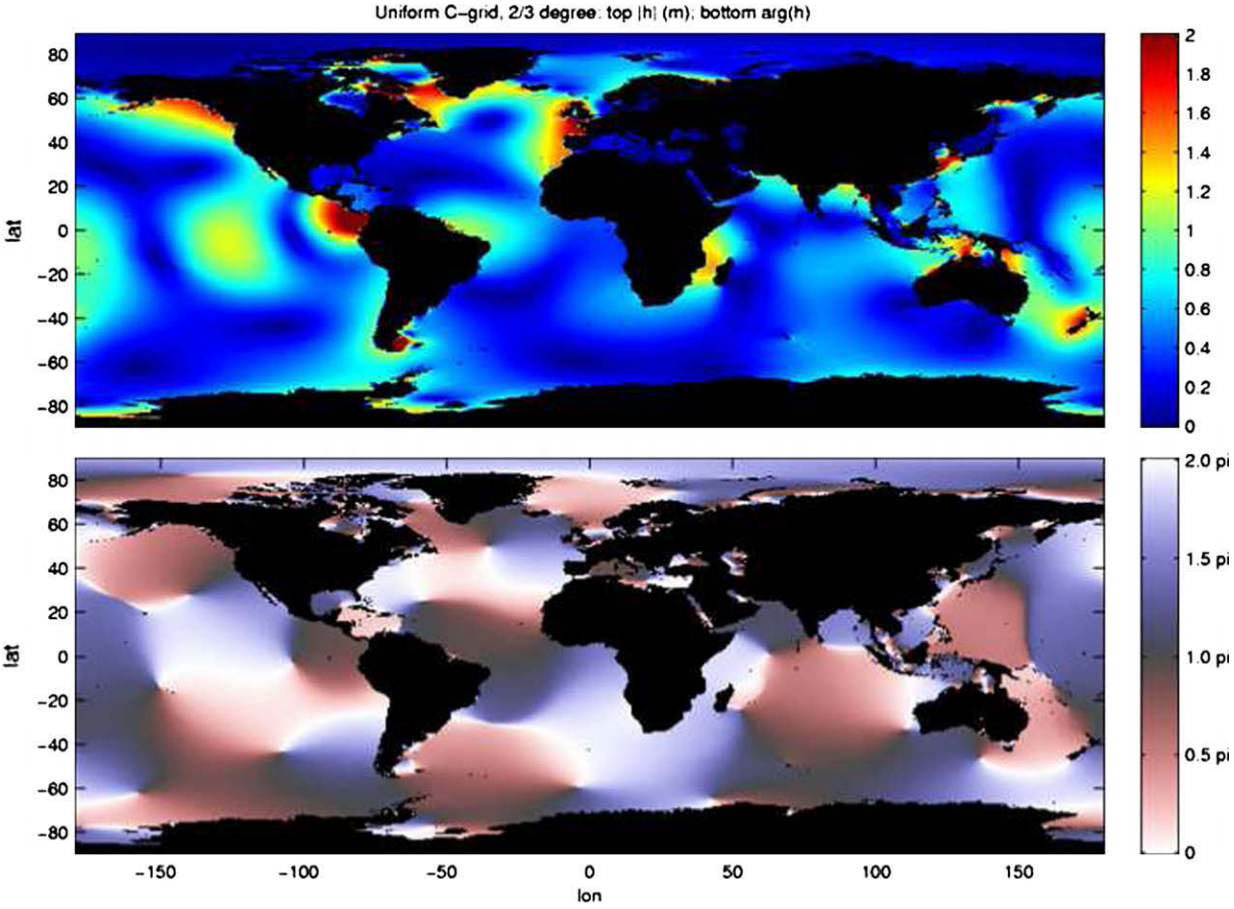

Fig. 4. Amplitude and phase plots from a regular grid tidal solution comparable to the unstructured grid results of Fig. 3. Physical parameters are identical and a 2/3° latitude–longitude grid makes resolution as similar as possible.

Please cite this article in press as: Stuhne, G.R., Peltier, W.R., An unstructured C-grid based method for 3-D global ocean dynamics: ..., Ocean Modell. (2009), doi:10.1016/j.ocemod.2008.11.005

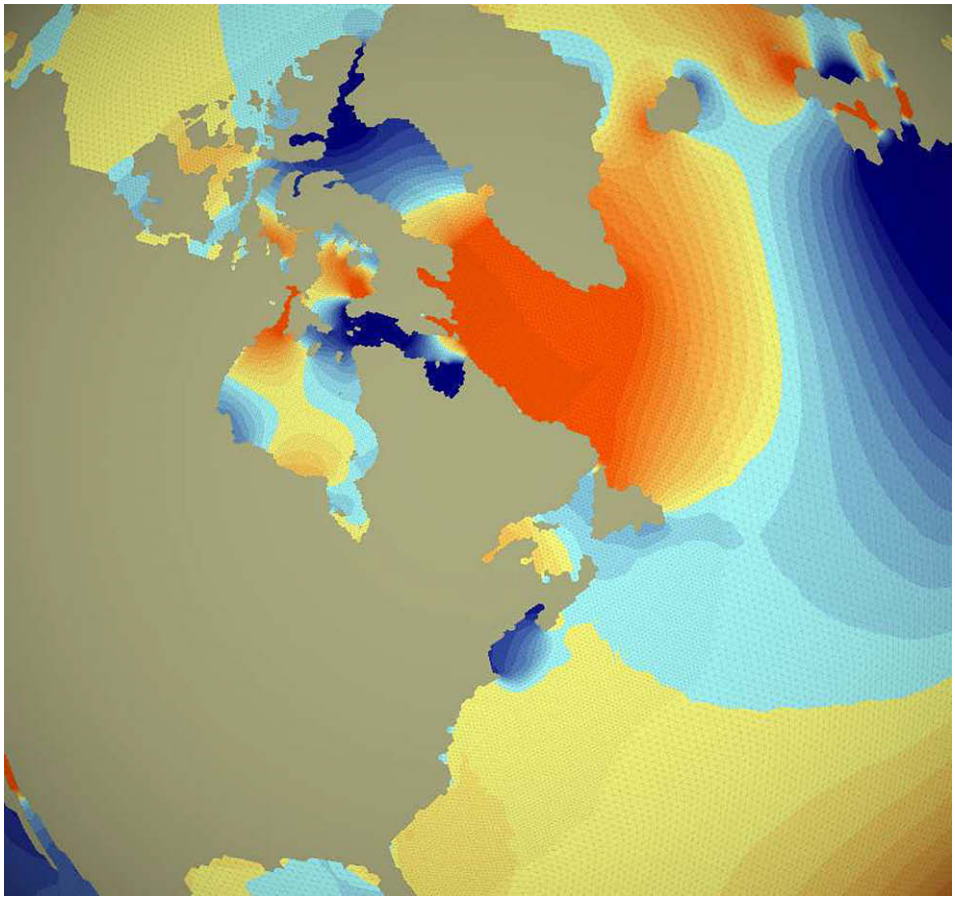

Fig. 5. Regional height displacement field from a tidal simulation identical to that of Fig. 3, apart from locally enhanced resolution in an area about Hudson's Bay. The illustrated mesh is enriched to level 8 and level 9 in two successive jumps, with the finest resolution being about 1/8°. Contours are spaced by 0.1 m/s in the range ±1 m/s.

of smoothing operations that can be used to avoid such problems through mesh optimization.

3.4. 3-D dynamics

Unstratified, hydrostatic 3-D dynamics are similar to shallow-water dynamics, except that our discretization replaces the continuous bottom topography with a "stair step" bathymetry defined by the prismatic z-coordinate system. The bottom frame of Fig. 6 shows the amplitude plot obtained after integrating the case of the previous subsection with the nonlinear model, a uniform level 7 horizontal grid, and a vertical discretization comprised of 10 levels of uniform 500 m thickness. The TOPEX/Poseidon observational data for the M_2 tide is shown in the top frame for comparison purposes, and comparison can also be made with the linear shallow-water case in Fig. 3. As should be expected, the 10 level vertical representation results in very poorly resolved coastal structures, but it can be seen that the deep ocean amphidromal patterns at least as good as in the shallow-water case. The same observations can be made from the tidal phase diagrams, which are shown in Fig. 7. Since we have not attempted to optimize and tune the parameterizations that were used, the actual fit to the TOPEX/Poseidon data is not a major issue.

It is clearly promising that the barotropic results are reproduced in 3-D geometry, and the next natural step is to consider the vertical structure of solutions. When vertical stratification is added to the initial conditions, the results, as expected, show the basic barotropic solution being non-trivially perturbed due to interactions with bottom topography. The energetics of density flows was considered in SP, and shown to be very well represented by the numerical scheme. In the present study, we did not go to high enough resolution to represent baroclinic wave generation by the barotropic tide, but small-scale results obtained by Fringer et al. (2006) using SUNTANS show that C-grid methods can, in principle, resolve the baroclinic tides. However, examination of the grids used by these authors show that they clearly have many more nodes per per baroclinic wavelength than were used by Simmons et al. (2004) in their regular grid simulations of the global baroclinic tide. So, we have to ask whether unstructured C-grid methods inherently need a substantially greater resolution than their regular grid counterparts, just to resolve the same physics.

Unfortunately, there is evidence to support the idea that large-scale, coarsely resolved C-grid simulations may be hindered by accuracy problems. In work described in a recent preprint, Danilov (2008) has specifically identified a computational mode that appears to result from a numerical asymmetry between the discretizations of divergence and curl. The energy-conserving character of our scheme theoretically precludes the possibility of any *exponentially growing* numerical instability, but an energetically stable solution can still break down into non-physical "noise." Evidence of this phenomenon appears in our 3-D free-surface simulations in Western boundary regions. As Danilov (2008) noted, the problem can be controlled (but not completely eliminated) by

Please cite this article in press as: Stuhne, G.R., Peltier, W.R., An unstructured C-grid based method for 3-D global ocean dynamics: ..., Ocean Modell. (2009), doi:10.1016/j.ocemod.2008.11.005

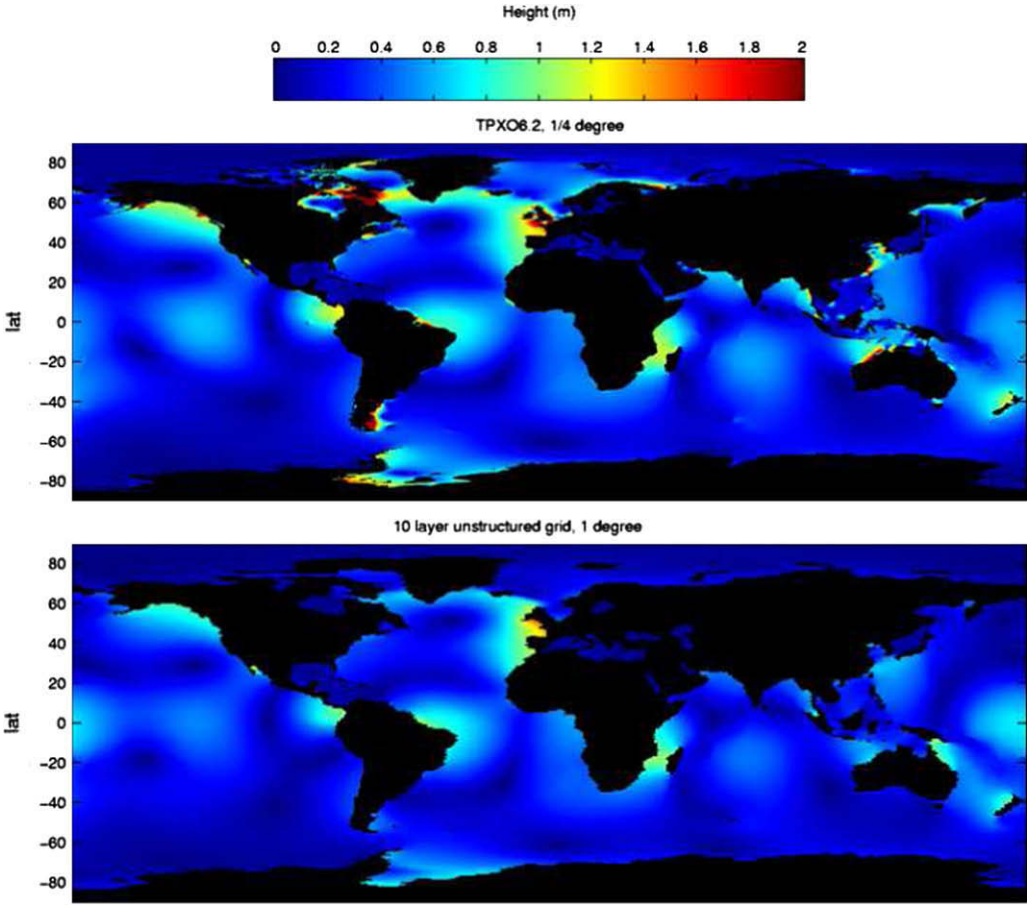

Fig. 6. Tidal amplitude plot from an equilibrated grid level 7 3-D SWM tidal simulation with 10 vertical levels (bottom). The top frame shows TOPEX/Poseidon data for comparison.

modifying the pressure field in the momentum equation as follows: i.e.,

$$p \to p - \nu_h^* \frac{\Delta^T(\ell u)}{A}, \tag{18}$$

which has the effect of introducing a diffusion of divergence into the dynamics. It naturally dissipates some of the physics of the solution as well, and this is one factor pointing to a need for extra resolution in the unstructured C-grid framework.

4. Conclusions

The unstructured grid numerical methodology presented in SP for rigid-lid global baroclinic ocean dynamics has been extended to shallow-water and 3-D free-surface dynamics. It performs well in the resolution of the barotropic tides, which are not affected by the unstructured C-grid computational mode. Other unstructured grid global shallow-water models have also been successfully applied to this problem (see, e.g. Carere and Lyard, 2003), which provides a useful baseline for more challenging test cases. In tandem with the previously published results in SP, the present work bridges the gap to global, coarsely-resolved 3-D simulations of the type relevant to climate modeling. Since we are among the first to go in this direction, there is little to compare with in the existing literature, and objective benchmarks need to be established to measure the relative advantages and disadvantages of unstructured and regular grid methods.

Overall, it has always been clear that regular grid techniques use computational resources more efficiently, when it comes to global simulations with more-or-less uniform grid resolution. With reference to these cases, the results herein and in SP suggest that the traditional methods may be more accurate as well, in the sense of requiring significantly less resolution to represent comparable physics. Even when the advantages of regular grids are compounded, however, there is theoretically a point at which the variable resolution capacity of unstructured grids should tip the balance in their favor. For the case of C-grid based finite-volume methods, the tipping point appears to be largely determined by the computational mode identified by Danilov (2008). The numerical methods are theoretically second-order accurate in the uniform grid limit, but the need to damp numerical "noise" can degrade the ideal properties.

It may be that an alternative unstructured grid numerical methodology will turn out to be more appropriate for global, coarsely-resolved simulations. Hall and Davies (2005), for example, used a local, high-resolution finite element model to resolve baroclinic dynamics associated with the tides. These authors, however, report artifacts arising from variable mesh resolution, and their plotted results do not look any better than the C-grid results of Fringer et al. (2006). One thing that should be agreed, however, is that the physics of the internal tides provides an ideal test case for the comparison and validation of global unstructured grid techniques. That leaves us with a challenge for future research.

Please cite this article in press as: Stuhne, G.R., Peltier, W.R., An unstructured C-grid based method for 3-D global ocean dynamics: ..., Ocean Modell. (2009), doi:10.1016/j.ocemod.2008.11.005

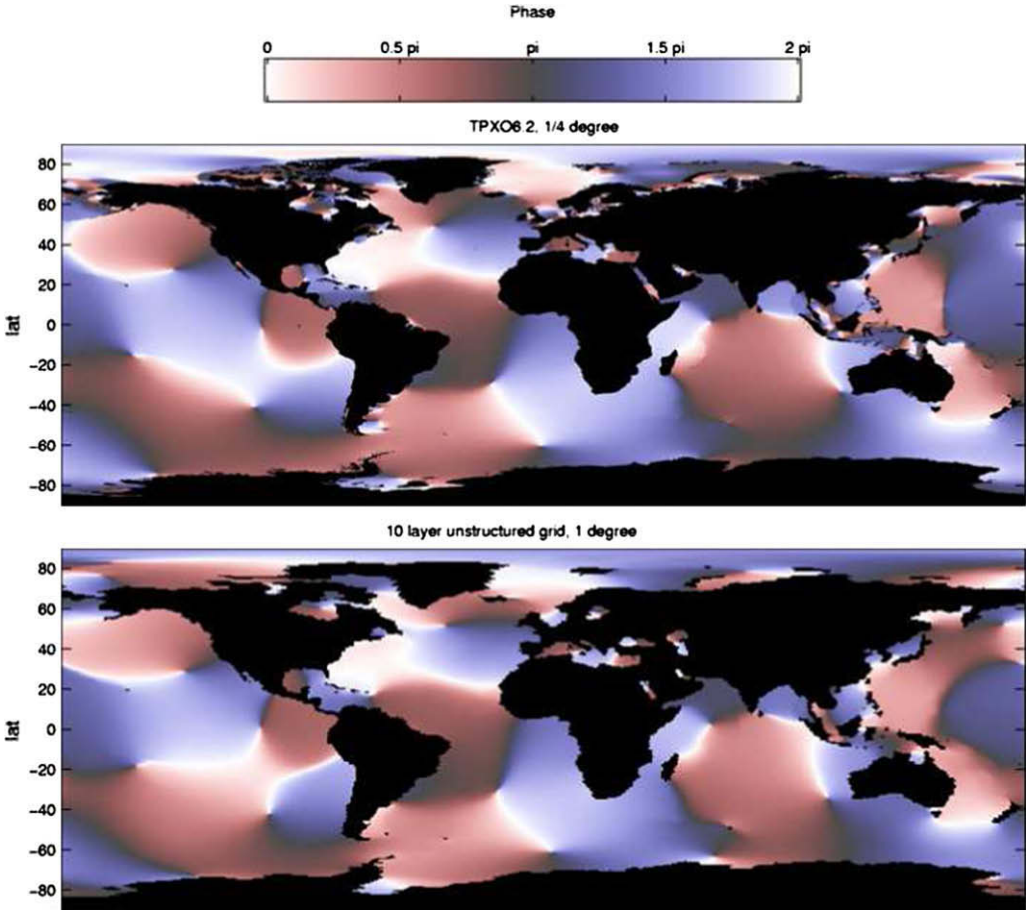

Fig. 7. Tidal phase plot from the case of Fig. 6, again compared with TOPEX data.

Acknowledgement

The work reported in this paper has been supported by the Polar Climate Stability Network which is financed by the Canadian Foundation for Climate and Atmospheric Sciences together with a consortium of Canadian Universities. The authors thank Stephen Griffiths for assistance with the generation of tidal amplitude-phase plots.

References

Arakawa, A., 1966. Computational design for long-term numerical integration of the equations of fluid motion: two-dimensional incompressible flow. Part I. J. Comput. Phys. 1, 119–143.

Bryan, K., 1969. A numerical model for the study of the world ocean. J. Comput. Phys. 4, 347–376.

Bryan, K., Cox, M.D., 1972. The circulation of the World ocean: a numerical study. Part I, a homogeneous model. J. Phys. Oceanogr. 2, 319–335.

Carere, L., Lyard, F., 2003. Modeling the barotropic response of the global ocean to atmospheric wind and pressure forcing – comparison with observations. Geophys. Res. Lett. 30, 1275.

Casulli, V., Walters, R.A., 2000. An unstructured grid, three-dimensional model based on the shallow water equations. Int. J. Numer. Methods Eng. 32, 331–348.

Chen, C., Liu, H., Beardsley, R.C., 2003. An unstructured grid, finite-volume, three-dimensional, primitive equations ocean model: application to coastal ocean and Estuaries. J. Atmos. Ocean. Tech. 20, 159–186 .

Cøté, J., 1988. A Lagrange multiplier approach for the metric terms of semi-Lagrangian models on the sphere. Quart. J.R. Met. Soc. 114, 1347.

Danilov, S., 2008. Numerical mode of unstructured triangular finite-volume discretization in quasi-geostrophic regimes, preprint.

Egbert, G.D., Ray, R.D., 2003. Semi-diurnal and diurnal tidal dissipation from TOPEX/Poseidon altimetry. Geophys. Res. Lett. 30, 1907.

Frayss, V., Giraud, L., Gratton, S., Langou, J., 2003. A Set of GMRES Routines for Real and Complex Arithmetics. Tech. Rep. TR/PA/03/3, CERFACS, public domain software available from: <www.cerfacs.fr/algor/Softs>.

Fringer, O.B., Gerritsen, M., Street, R.L., 2006. An unstructured-grid, finite-volume, nonhydrostatic, parallel coastal ocean simulator. Ocean Modell. 14, 139–173.

Gill, A.E., 1982. Atmosphere-Ocean Dynamics. Vol. 30 of International Geophysics Series. Academic Press, San Diego.

Griffiths, S.D., Peltier, W.R., 2008. Polar ocean tides at the last glacian maximum: amplification, sensitivity, and climatological implications. J. Climate, in press, doi:10.1175/2008JCLI2540.1.

Hall, P., Davies, A.M., 2005. Comparison of finite difference and element models of internal tides on the Malin-Hebrides shelf. Ocean Dynam. 55, 272–293.

Lynch, D.R., Ip, J.T.C., Naimie, C.E., Werner, F.E., 1996. Comprehensive coastal circulation model with application to the Gulf of Maine. Cont. Shelf Res. 16, 875–906.

Murray, R.J., 1996. Explicit generation of orthogonal grids for ocean models. J. Comput. Phys. 126, 251–273.

Myers, P.G., Weaver, A.J., 1995. A diagnostic barotropic finite-element ocean circulation Model. J. Atmos. Ocean. Tech. 12, 511–526.

National Geophysical Data Center (NGDC), 2001. 2-Minute Gridded Global Relief Data (ETOPO2). Available from: <www.ngdc.noaa.gov/mgg/global/relief/ETOPO2>.

Nechaev, D., Schröter, J., Yaremchuk, M., 2003. A diagnostic stabilized finite-element ocean circulation model. Ocean. Modell. 5, 37–63.

Perot, B., 2000. Conservation properties of unstructured staggered mesh schemes. J. Comput. Phys. 159, 58–89.

Simmons, H.L., Hallberg, R.W., Arbic, B.K., 2004. Internal wave generation in a global baroclinic tide model. Deep Sea Res. 51, 3043–3068.

Stuhne, G.R., Peltier, W.R., 2006. A robust unstructured grid discretization for 3-dimensional hydrostatic flows in spherical geometry: A new numerical structure for ocean general circulation modeling. J. Comput. Phys. 213, 704–729.

Zhang, Y., Baptista, António M., Myers, E.P.I., 2004. A cross-scale model for 3D baroclinic circulation in estuary-plume-shelf systems: I. Formulation and skill assessment. Cont. Shelf Res. 24, 2187–2214.